Continental Shelf Research 28 (2008) 1246–1260

Contents lists available at ScienceDirect

Continental Shelf Research

journal homepage: www.elsevier.com/locate/csr

Topographic effects on the anticyclonic vortex evolution: A modeling study

Kyung Hoon Hyun [a,*], Patrick J. Hogan [b]

[a] Department of Marine Sciences, University of Southern Mississippi, Stennis Space Center, MS 39529, USA
[b] Naval Research Laboratory, Stennis Space Center, MS 39529, USA

ARTICLE INFO

Article history:
Received 22 March 2007
Received in revised form
6 December 2007
Accepted 14 February 2008
Available online 4 March 2008

Keywords:
Anticyclonic vortex
Topographic effect
HYCOM
Slope steepness and orientation

ABSTRACT

The evolution of anticyclonic vortices in the presence of topographic effects associated with continental slope steepness and orientation is investigated using the Hybrid Coordinate Ocean Model. The trajectories of the vortices are analyzed using various configurations of slope steepness and orientation, including a flat bottom. As the steepness of the slope is increased, the development and evolution of a counter-rotating subsurface vortex ('deep cyclone') is strongly dispersive resulting in strong zonal translation over the slope, although the translation is southwest with a coherent deep cyclone, in the flat bottom case. In particular, the zonal translation is faster with a gentle slope (relative to the flat bottom case) due to an upslope tilt of the deep cyclone. As the surface vortex collides with the steep topography, the deflection angle increases as the slope increases (i.e. it deflects along slope) at the same time the bottom vorticity peaks, generating a 'collision' cyclone and a slope jet south of the vortex-slope impact. In the realistic steep slope case, along slope translation is dominant when the vortex departs over/near the slope, although the vortex strongly collides with (and rapidly crosses) the slope if it has strong westward inertia. During the cross-slope translation, vorticity restoration by vortex compression occurs with relatively small poleward translation. At the point of maximum bottom vorticity, rapid vortex erosion occurs horizontally and vertically, and southwestward translation is restored. Comparison of vortex translation over four different slope orientations suggests that the vortex is strongly affected by the location of adjacent cyclones which tend to propagate onshore and poleward simultaneously, and that the combined planetary and topographic β-effect slows the vortex translation on the northern slope.
Published by Elsevier Ltd.

1. Introduction

Ubiquitously distributed oceanic vortices translate mainly westward due to the planetary β effect (Warren, 1967; McWilliams and Flierl, 1979; Robinson, 1983; Kamenkovich et al., 1986), encounter slopes/hills/ridges or depressions/canyons and undergo major changes of their translation (speed, direction) and intensity/dissipation due to topographic effects (Kamenkovich et al., 1996). Typical examples of these vortices experiencing topographic interactions are the Loop Current Eddies (Hurlburt and Thompson, 1980; Vidal et al., 1992), the Gulf Stream rings (Cheney and Richardson, 1976), the Kuroshio warm core rings (Matsuura and Kamachi, 1993), the North Brazil Current Rings (Fratantoni et al., 1995), the Gulf of Alaska Eddies (Ladd et al., 2005), Agulhas Rings (Byrne et al., 1995), Meddies (Wang and Dewar, 2003), etc.

Vortex–topography interactions have been widely investigated by observation (e.g. Vukovich and Waddell, 1991), analytical/numerical models (Nof, 1983; Smith and O'Brien, 1983; Grimshaw et al., 1991; Sutyrin et al., 2003) and laboratory experiments (Mory et al., 1987; Whitehead et al., 1990; Carnevale et al., 1991). Specific examples of numerical modeling research include the western boundary effect (Shi and Nof, 1993; Nof, 1999), influence of a strong bottom slope (Thierry and Morel, 1999), the effect of the shelf/slope width (Frolov et al., 2004), vortex erosion (Herbette et al., 2003, 2005) and generation of a strong subsurface slope jet (Oey and Zhang, 2004). Louis and Smith (1982) documented the generation of topographic Rossby waves by a Gulf Stream ring approaching the Scotian Shelf. Gulf Stream rings have been observed to pass over the New England seamounts, and propagate onto the continental shelf/slope regions (Cheney and Richardson, 1976). Brown et al. (1986) suggested that ring–shelf interaction is a significant factor influencing Gulf Stream ring evolution, and that anticyclones have difficulty crossing the slope and shelf break due to the tendency of down slope drift by topographic β. Smith (1986) investigated vortex–topography interaction using a two-layer primitive equation model, and reported the "reflection" of anticyclones in conjunction with strong lower layer currents along the western slope of the Gulf of Mexico (GoM). Fratantoni et al. (1995) investigated the Northern

* Corresponding author. Tel.: +1 228 688 5907; fax: +1 228 688 5997.
E-mail addresses: hoon.hyun@gmail.com (K.H. Hyun), hogan@nrlssc.navy.mil (P.J. Hogan).

0278-4343/$ - see front matter Published by Elsevier Ltd.
doi:10.1016/j.csr.2008.02.011

Brazil Current (NBC) rings using hydrographic, current and satellite data including the Coastal Zone Color Scanner, and reported that NBC rings transport ~20% of the total meridional heat transport northwestward following the northeastern continental slope of South America.

Despite numerous studies of vortex–topography interaction, studies on the effect of the slope steepness and orientation have been rare. Jacob et al. (2002) questioned whether vortex baroclinicity/barotropicity affected vortex–topography interactions and what the influences of topographic orientation were, and suggested that vortex propagation over a slope strongly depended on the barotropicity of the vortex, the orientation and steepness of the slope, and that a northward-sloping topography increased the propagation speed because both the planetary and topographic β effects were in the same direction, whereas a southward-sloping slope decreased the speed. Sutyrin et al. (2003) investigated the Loop Current Eddy (LCE) translation over an idealized northwestern GoM slope using a two-layer model, and reported that a deep cyclone near the trailing edge of an upper vortex accelerated southward translation, and that a northward translation along the western boundary was induced by the 'image' effect. Frolov et al. (2004) investigated the effects of two typical configurations of slope geometry in the western GoM (wide shelf-narrow slope/narrow shelf-wide slope) on the LCE–topography interaction, and showed that a southward translation occurred on both slopes with an oscillated cyclic trajectory but the cyclic motion was critically controlled by the slope width. Herbette et al. (2003, 2005) investigated the vortex erosion over a sea mount using f- and β-planes, and suggested that the deep fluid motions induced by the initial vortex played a major role in the erosion.

In this paper, vortex–topography interactions are investigated using a multi-layered version of the Hybrid Coordinate Ocean Model (HYCOM). Specific topics examined include how the slope steepness and orientation affects vortex evolution ("vortex" indicates anticyclonic vortex hereafter) on f- and β-planes, how zonal/meridional translation changes with steepness, orientation and the presences of a deep current, and how the vortex collision against topography changes the vortex evolution. Slope configurations include a flat bottom, two linearly sloping bottoms and a steep topography (representing a realistic shelf-slope front). Also examined are whether the vortex translates cross-slope or along slope over the steep slope, how the vortex erosion occurs due to the collision of the vortex, and the effect of the initial distance from the slope and the vorticity variation over steep topography.

The paper is organized as follows: Section 2 explains the details of model, model topography and vortex initialization. Section 3 describes the results from numerical experiments of the vortex evolution with various topographic configurations. The effects of the steepness on f- and β-planes are described in Section 3.1. The effect of the slope orientation is described in Section 3.2. In Section 3.3, vortices along slope deflection by vortex collision against a steep topography is described. The vortex evolution over a steep slope is discussed in Section 3.4, including the effect of the initial location from the slope, the strong vortex collision/erosion, and the vorticity variation of the vortex crossing the slope. Concluding remarks are given in Section 4.

2. Method

For this study, HYCOM is used to examine vortex–topography interactions using idealized topographic configurations. HYCOM is a currently state of the art community ocean model with several choices for vertical grid representation and parameter space options [refer to Bleck and Boudra (1981); Bleck (2002); Chassignet et al. (2007) for details]. This research was motivated from the interactions between LCE and the continental slopes. An idealized model with the same GoM circulation model setup, including thin surface hybrid layers and reference density at each layer, was suggested for this research, in order for an isolated vortex to be as analogous as possible to LCE. For the simulations in this study, 14 hybrid layers are used in the vertical, and the horizontal grid resolution is 1/20 (~5 km). Lateral boundaries are closed (no-slip boundary condition) and there is no surface boundary forcing. Initial stratification was obtained from mean January temperature and salinity profiles averaged over each layer in the entire GoM model domain from the GDEM3 climatology (Teague et al., 1990). The stratification is spatially uniform over the model domain except within the implanted vortex structure.

Using the HYCOM configuration described above, a suitable methodology for initializing geostrophically balanced anticyclones was sought. The method chosen for this study follows that of Carton and Williams (1989) and Herbette et al. (2003). In polar coordinates, the system to solve is

$$\frac{v_k^2}{r} + f v_k = \frac{\partial M_k}{\partial r},$$

$$\varsigma_k - f\frac{\Delta h_k}{H_k} = \Delta Q_k\left(1 + \frac{\Delta h_k}{H_k}\right),$$

where ς_k is the relative vorticity in polar coordinates, k is the layer subscript, v_k is the azimuthal velocity, M_k is the Montgomery potential, $\Delta h_k = h_k - H_k$ is the layer thickness variation where H is the layer thickness at rest, h is the layer thickness, and f is the Coriolis parameter of $7.0\times10^{-5}\,\mathrm{s}^{-1}$. This system of partial differential equations is non-linear because of the quadratic term associated with the centrifugal force v_k^2/r. By assuming geostrophic equilibrium, the centrifugal force term is absent from the equations, and the system can be solved with the boundary conditions that the layer thickness difference between the vortex and the ambient water at rest is zero at the vortex perimeter, and the azimuthal velocity is zero at the vortex center. Using this method, the potential vorticity anomaly (PVA, ΔQ_k), defined as

$$\Delta Q_k = H(\zeta + f)/h - f/h,$$

decreases with the distance from the vortex center according to

$$\Delta Q^0_{k,r} = \Delta Q^0_{k,0}(1 - r^2/R^2)\mathrm{e}^{-(r/R)\hat{}2},$$

where k is the layer and r the distance from the center. The initial vortex diameter ($2R$) is 150 km. The initial PVA ($\Delta Q^0_{(k\,=\,1\text{–}10, r\,=\,0)}$) of $-1.0f$ is given in layers 1–10, and zero PVA is prescribed for the bottom four layers ($\Delta Q^0_{(k\,=\,11\text{–}14)} = 0$) to minimize the lower layer flow. The vertical structure of the initial swirl speed and the layer thickness is depicted in Fig. 1. Maximum surface flow is $\sim 40\,\mathrm{cm\,s}^{-1}$ near the surface, which is typical of anticyclonic eddies observed in the western GoM (Kirwan et al., 1988). The vortex initialization procedure of Herbette et al. (2003) was developed to apply for a flat bottom ocean. In the cases that include a slope configuration, the vortex initialization process generated deep transient currents near the bottom, but these currents were small and deemed to have little effect if any on the results.

The model domain is $1015\times1000\,\mathrm{km}^2$ and bounds the area 82–92°W and 24–33°N. Four topographic configurations with different steepness were generated; a flat bottom, a weak linear slope, an intermediate linear slope and a tapered steep slope (Fig. 2). The configurations with a weak and intermediate linear slope have a tilt across the bottom over the entire domain, whereas the configuration with the tapered steep slope has a flat bottom in the abyssal regions, i.e. east of 88°W (Fig. 2). Slope parameters β_τ ($= f\,\mathrm{d}h/h\mathrm{d}x$) and case descriptions are given in

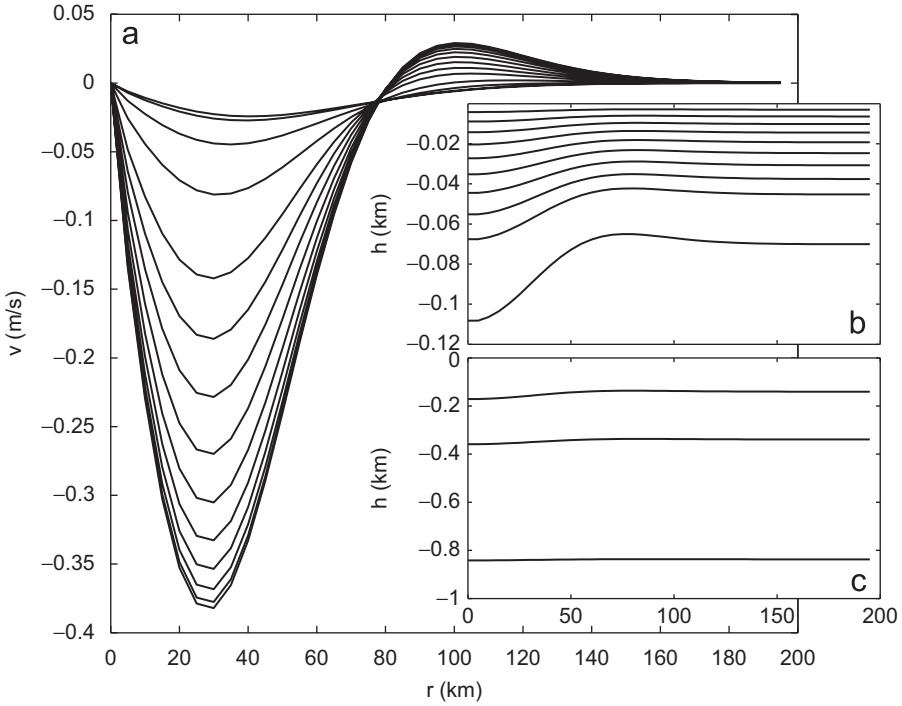

Fig. 1. (a) The swirl speed and (b) (c) the layer interface depth of the initial vortex. (b) Layers 1–10 and (c) layers 11–14 are depicted for the eastern half of the vortex (r is the radius from the center).

Table 1. The steep slope configuration is slightly gentler than the observed GoM slope ($\beta_\tau = 31 \times 10^{-11}\,\mathrm{m^{-1}\,s^{-1}}$). The shelf break is located 100 km offshore from the western boundary and the width of slope is 100 km. A relatively wide shelf was used to minimize the effects of the closed boundaries. The depth ranges 100–1000 m from the shelf to the abyssal ocean. A total of 13 simulations were performed and integrated for two model years. Cases F0–F3, B0, W1–W3 were performed to investigate the effect of the slope steepness with/without planetary β effect. Three experiments with the steep slope configuration (W3–W5) were performed with different initial location from the slope (Fig. 2d). W3 was initialized over the slope; W4 near the slope but over the abyssal flat bottom; W5 was initialized over the abyssal flat bottom far from the slope. To investigate the effect of the slope orientation, eastern/southern/northern slope configurations with the intermediate steepness (Cases E2/S2/N2) were compared with the western intermediate slope case (W2) and flat bottom (B0).

3. Result

3.1. Effect of the slope steepness

In this section, the impact of slope steepness is examined. In cases F1–F3, which used the f-plane approximation, the vortex translated down slope in all cases, but after initial down slope translation, the vortex became stationary immediately after it detached from the slope in cases F2, F3 (Fig. 3). LaCasce (1998) investigated a cyclonic vortex over a slope using an f-plane with a two-layer model and suggested that over steeper slopes, the vortex separated into topographic waves and a stationary surface-trapped vortex. This study shows that the basic translation mechanism between cyclone and anticyclone is analogous, except that they translate in opposite direction. Our experiments with an f-plane demonstrate that larger topographic β causes stronger topographic Rossby waves, which not only result in rapid initial down slope drift but also a rapid evolution into a 'compensated' state (zero deep flow). During this process, a cyclone is generated north of the vortex by the topographic β effect ('β_τ cyclone' hereafter). Over the steeper slope configurations (F2, F3), another cyclone is generated south of the vortex by the collision of the onshore flow component of the vortex against the slope.

Cases F0–F3, described in the previous paragraph, were repeated using the β-plane approximation. These are B0 (flat bottom), W1 (weak slope), W2 (intermediate slope) and W3 (steep slope) (Table 1). Fig. 4 shows that all exhibit south-westward translation. The zonal speed is $\sim$0.5 km day^{-1} in the flat bottom case (B0) and analogous to the long Rossby wave phase speed of 0.56 km day^{-1} ($=\beta R_d^2$, R_d is internal Rossby radius), which is consistent with the results from a two-layer primitive equation model by Mied and Lindemann (1979) and a quasi-geostrophic model by McWilliams et al. (1986). They reported that the westward translation speed increased toward βR_d^2 with southward translation at a maximum of 1/4 βR_d^2. Our result suggests that the zonal translation is independent of vortex strength (by presuming the vortex decays with time), which is consistent with results from reduced gravity models (e.g. Nof, 1983; Jacob et al., 2002). W1 exhibits the fastest zonal translation and W3 the slowest (W1 > B0, W2 > W3). The meridional translation is the fastest in B0 but slowest in W3 (B0 > W1 > W2 > W3). In the slope cases W1–W3, the zonal/meridional translation decreases as the slope increases. Slower translation over steeper slopes can be attributed to stronger topographic constraint. However, the faster zonal translation in the weak slope case (W1) relative to the flat bottom case (B0) is counter intuitive to the conventional idea that topography hinders the vortex from drifting upslope. Note also that the zonal translation in W2 is close to that in B0 despite the topographic constraint. Recall that most observed ocean vortices have a dominant zonal drift with a very slow meridional drift (e.g. Morrow et al., 2004), and that the ocean is not flat even though numerous model experiments exhibited a substantially strong meridional translation over a flat bottom (Sutyrin et al., 2003;

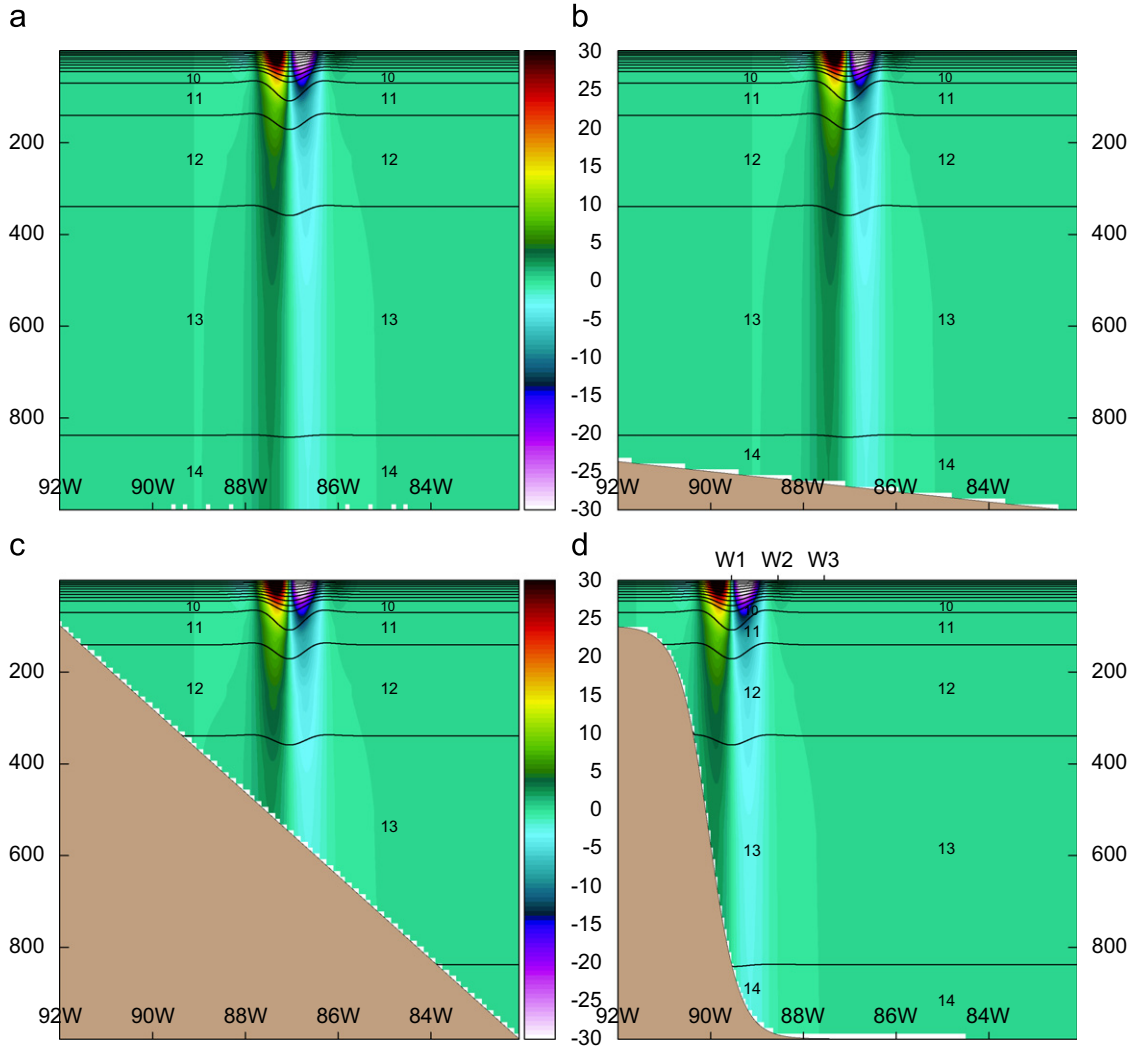

Fig. 2. Cross-sections of current speed through the center of the initial vortex over (a) a flat bottom, (b) a weak slope, (c) an intermediate slope and (d) a steep slope. The initial location is the center of domain (87.1°W/28.7°N) for the flat and linearly sloping bottoms. For the steep slope, the vortex is initialized at 89.6°W, 88.6°W, 87.6°W along 28.7°N for cases W1, W2, W3, respectively. Color bar denotes flow speed (cm s^{-1}).

Table 1
List of simulations: the topographic beta (β_τ) is calculated as $\beta_\tau = f/h\,dh/dx$ (m^{-1} s^{-1}), where f is 0.7×10^{-4} s^{-1} and h is 1000 m

Case	β_0	β_τ	Initial location	Configuration
F0	0	0	Center	Flat
F1	0	1	Center	Western
F2	0	7	Center	Western
F3	0	31	89.6°W	Western
B0	2	0	Center	Flat
W1	2	1	Center	Western
W2	2	7	Center	Western
W3	2	31	89.6°W	Western
W4	2	31	88.6°W	Western
W5	2	31	87.6°W	Western
N2	2	7	Center	Northern
S2	2	7	Center	Southern
E2	2	7	Center	Eastern

The planetary (β_0) and topographic beta (β_τ) have units of 10^{-11} m^{-1} s^{-1}. The initial location of the vortex is the center of domain (87.1°W/28.7°N), for the flat and linearly sloping bottoms. For the steep slope cases (W3/W4/W5), the vortex is initialized at 89.6°W, 88.6°W, 87.6°W along 28.7°N, respectively.

Herbette et al., 2005). Chassignet and Cushman-Roisin (1991) suggested that reduced gravity approximation, which assumed an infinitely deep lower layer at rest, was only valid for vortices smaller than the deformation radius. However, most major oceanic eddies are generally larger than the deformation radius (typically O (100) km) but still have dominant zonal translation. This phenomenon can be explained by the topographic effect, which accelerates the dispersion of subsurface cyclones and a tendency to tilt upslope as described below.

Fig. 5 depicts vortex evolution over a flat bottom and three slope configurations at day 300. As depicted by the vortex trajectory, B0, W1, W2 translate southwestward continuously, and W3 translates almost due southward (along slope). Case B0 exhibits the typical drift pattern of an anticyclonic vortex on a β-plane flat bottom configuration (Fig. 5a). It is well known that vortices propagate westward due to Rossby wave dispersion (Flierl, 1977, 1984) and southward through non-linear (NL) advective processes (McWilliams and Flierl, 1979; Smith and Reid, 1982; Flierl, 1984; Nof, 1983). In general, a dipole (anticyclone–cyclone pair) generated by the "β-gyre" dynamics (LaCasce, 1998) transforms into a modon as the vortex translates southwestward and the trailing Rossby wake northeastward. Note that a planetary Rossby wave pattern is seen toward the northeast from the vortex core (i.e. the repetition of anticyclone–cyclone–anticyclone in Fig. 5a). W1 is analogous to B0 except that adjacent cyclonic vortices are strongly dispersive (Fig. 5b), unlike the other cases, such as the steep slope configurations (W2/W3), and the flat

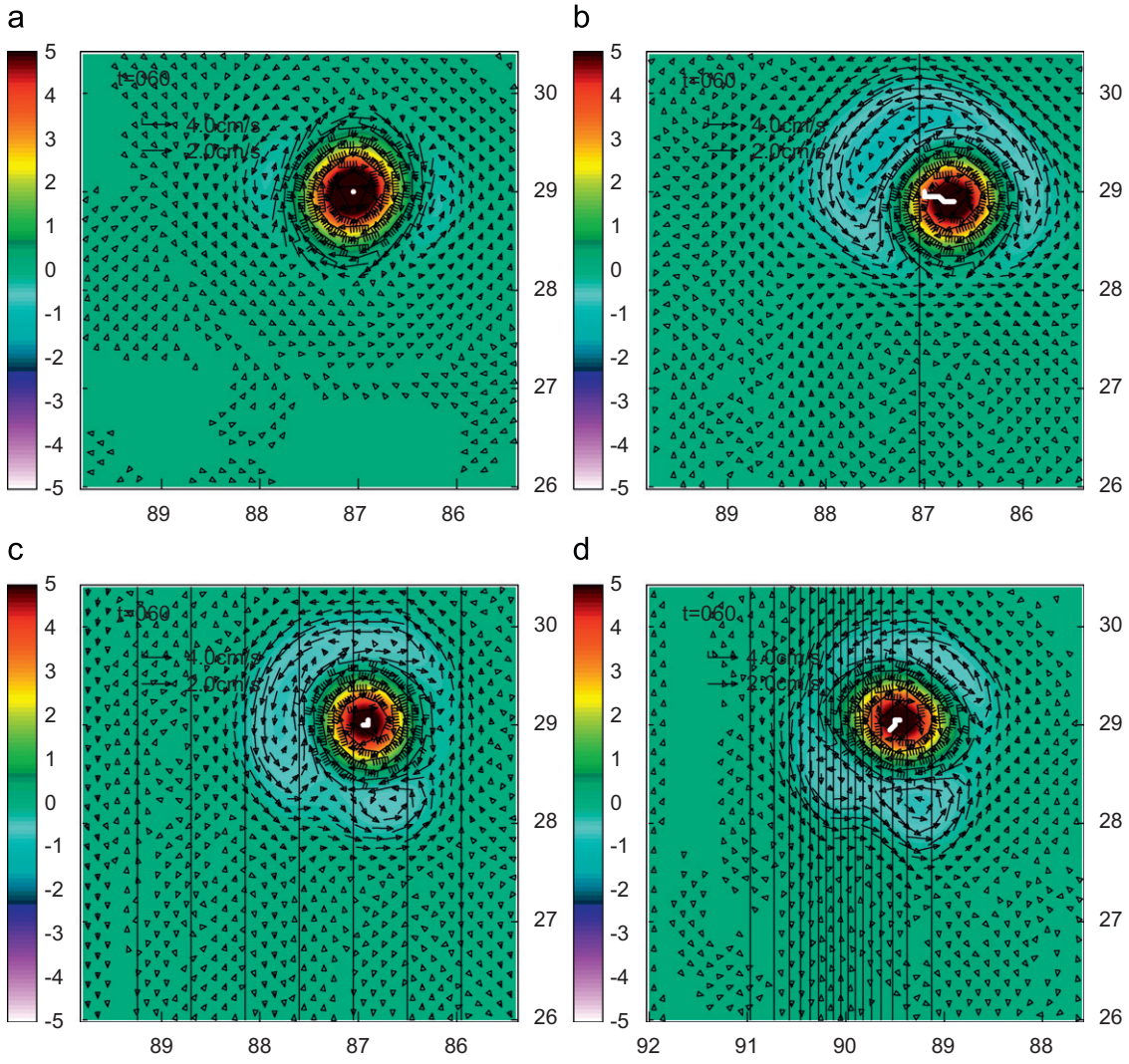

Fig. 3. Vortex behavior with *f*-plane over (a) a flat bottom, (b) a weak slope, (c) an intermediate slope and (d) a steep slope at 60 days. Layer 10 currents are shown as vectors, the SSH (cm) is shown as color, and the trajectory of the vortex center is shown as a white line. Bathymetry is superimposed every 50 m.

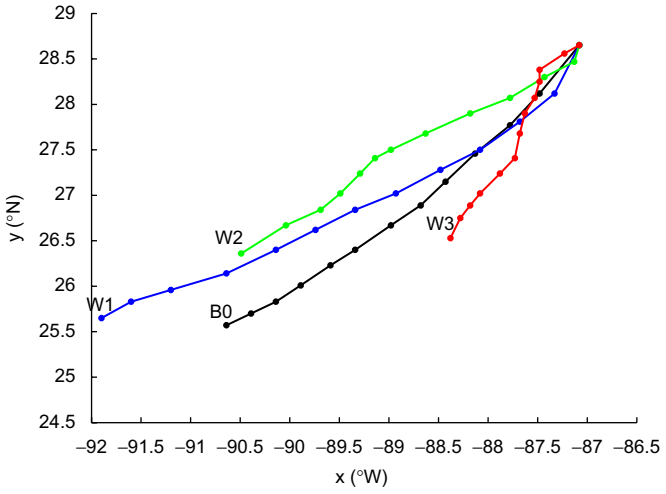

Fig. 4. Vortex trajectory with β plane over the flat bottom, weak, intermediate and steep slopes (cases B0/W1/W2/W3) for 2 years. The location of the vortex center is denoted as solid dots at every 60 days for 720 days.

bottom case (B0), in which the cyclone located north of the vortex is less dispersive (Fig. 5c, d). The enhanced dispersion in W1 can be attributed to a gently sloping bottom (small topographic β effect), which initially generates a dispersive β_τ cyclone north of the vortex on an *f*-plane (Fig. 3b). On the other hand, over steeper slope configurations, the adjacent cyclone is more coherent and less dispersive, which suggests that steeper slope configurations stabilize the surface vortex (LaCasce, 1998). Also, in the intermediate slope case (Fig. 5c), the meridional translation is much reduced relative to B0, W1, and in W3, the vortex translates primarily in the zonal direction for the first 150 days, after which it turns and propagates along slope (see trajectory in Fig. 5d). Thus, it is suggested that the vortex has a larger westward component of translation as the steepness increases, until the vortex deflects along slope by the slope (details in Section 3.3).

Fig. 6 depicts the zonal section along the vortex center at day 300 corresponding to Fig. 5. For the flat bottom case (B0), the vortex becomes surface trapped (above 300 m), and the barotropic 'β_0 cyclone' east of the vortex (not shown) is isolated in layer 13 at ~600 m ('deep cyclone' hereafter) (Fig. 6a). Note a southward flow beneath the center of the upper vortex and a northward flow east

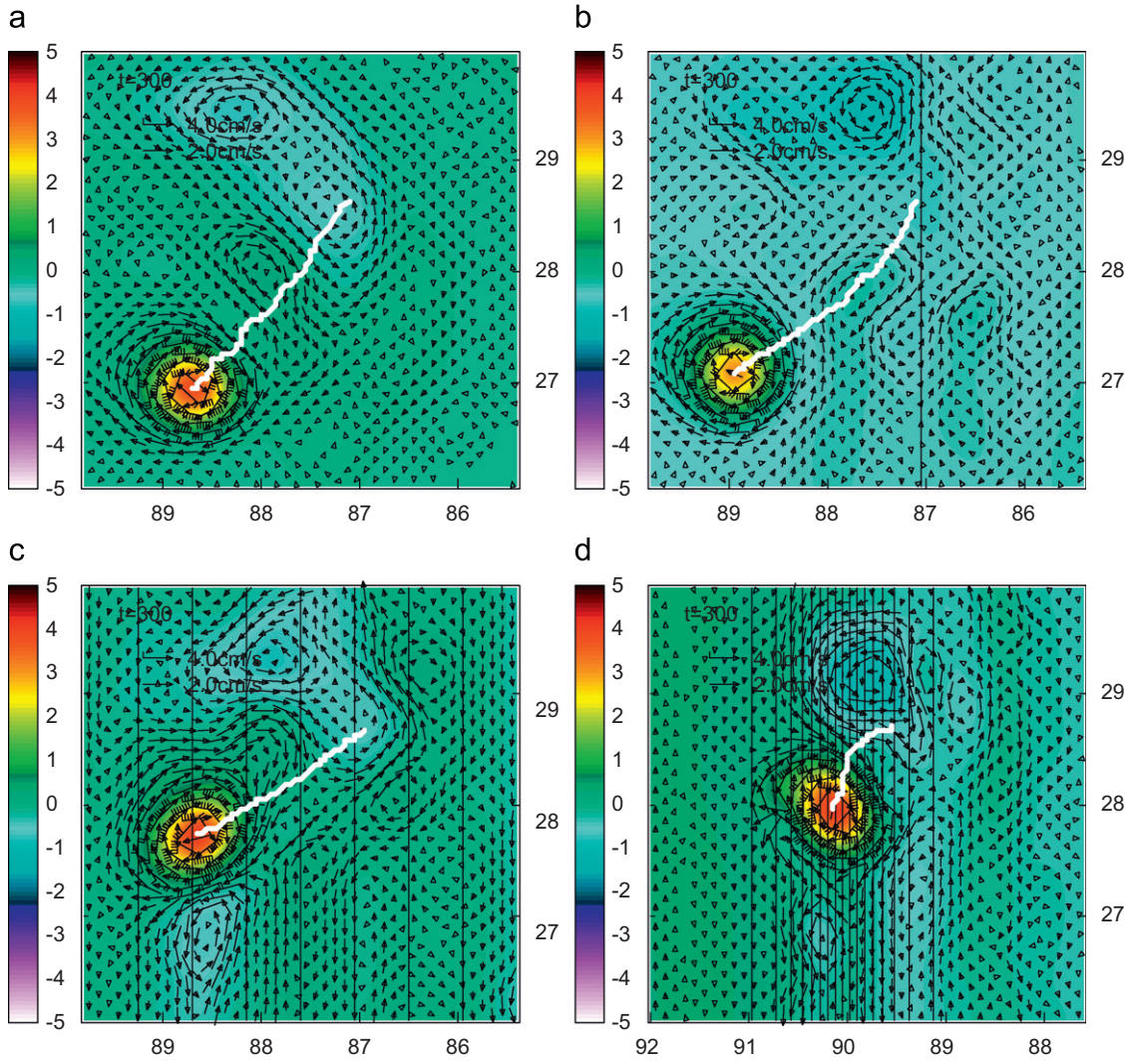

Fig. 5. β-Plane vortex evolution after 300 days for (a) a flat bottom, (b) a weak slope, (c) an intermediate slope and (d) a steep slope (cases B0, W1, W2, W3, respectively). Subsurface current (layer 10), SSH (cm) and trajectory of the vortex center are depicted. Bathymetry is superimposed every 50 m.

of the vortex in layer 13. Sutyrin et al. (2003) suggested that southward vortex translation was strongly accelerated by the deep cyclone, and decreased as the deep cyclone dispersed over the slope. For the weak slope case (W1), the vortex is weaker (more dissipative) than B0 and the deep cyclone tilts slightly upslope in layer 14 and its center shoals to ~300 m (Fig. 6b). The southward flow of the deep cyclone beneath the upper vortex is weaker, but the northward branch of the deep cyclone is stronger relative to B0, which causes a slower meridional translation than B0. However, for the intermediate slope case (Fig. 6c), the onshore part of the vortex extends to the bottom, and the signature of the deep cyclone is largely restricted to layer 12, indicating rapid dissipation of the deep cyclone over steeper slopes. The upslope tilt of the lower layer vortex (remnant of the deep cyclone) is still seen in W2 after 300 days. In the steep slope case (W3), the vortex is horizontally compressed and the onshore side of the vortex in layer 12 directly interacts with the slope, generating a cyclonic circulation between the vortex and the shelf edge, which is a signature of vortex collision with topography. During the subsequent along slope translation, another subsurface cyclone emerges east of the vortex in layer 12 (Fig. 6d), which suggests linkage with the southward translating surface vortex and the coherent subsurface cyclone.

The relationship between the zonal/meridional translation and the deep current structure for B0 and W1 is described below. Fig. 7 depicts the volume translation speed integrated inside of the vortex at each depth. For the flat bottom case, the zonal translation does not have a significant difference with depth (Fig. 7a), i.e. the zonal speed of ~0.2 km day^{-1} is persistent at each depth but decreases with time due to dissipation (~0.1 km day^{-1} at day 300). The zonal volume translation speed is less than the actual vortex translation (obtained from the trajectory of the vortex center), suggesting that the zonal translation is affected by surrounding ocean conditions such as Rossby wave propagation. For the meridional translation (Fig. 7b), the surface vortex above 50 m does not show significant southward translation, but the deep vortex exhibits a strong southward translation (0.4–0.8 km day^{-1} below 500 m in Fig. 7b). This result indicates that the deep current is an important source for the vortex meridional translation. The zonal/meridional translation is strongly modified by the deep current in the weak slope case (Fig. 7c, d). The zonal translation increases with time beneath 250 m (Fig. 7c), and faster than the flat bottom case after ~100 days (0.4 km day^{-1} vs. 0.2 km day^{-1} at day 300). The meridional translation in W1 decreases rapidly compared to B0 (see Fig. 7b, d). In the intermediate slope case (W2, not shown), the volume

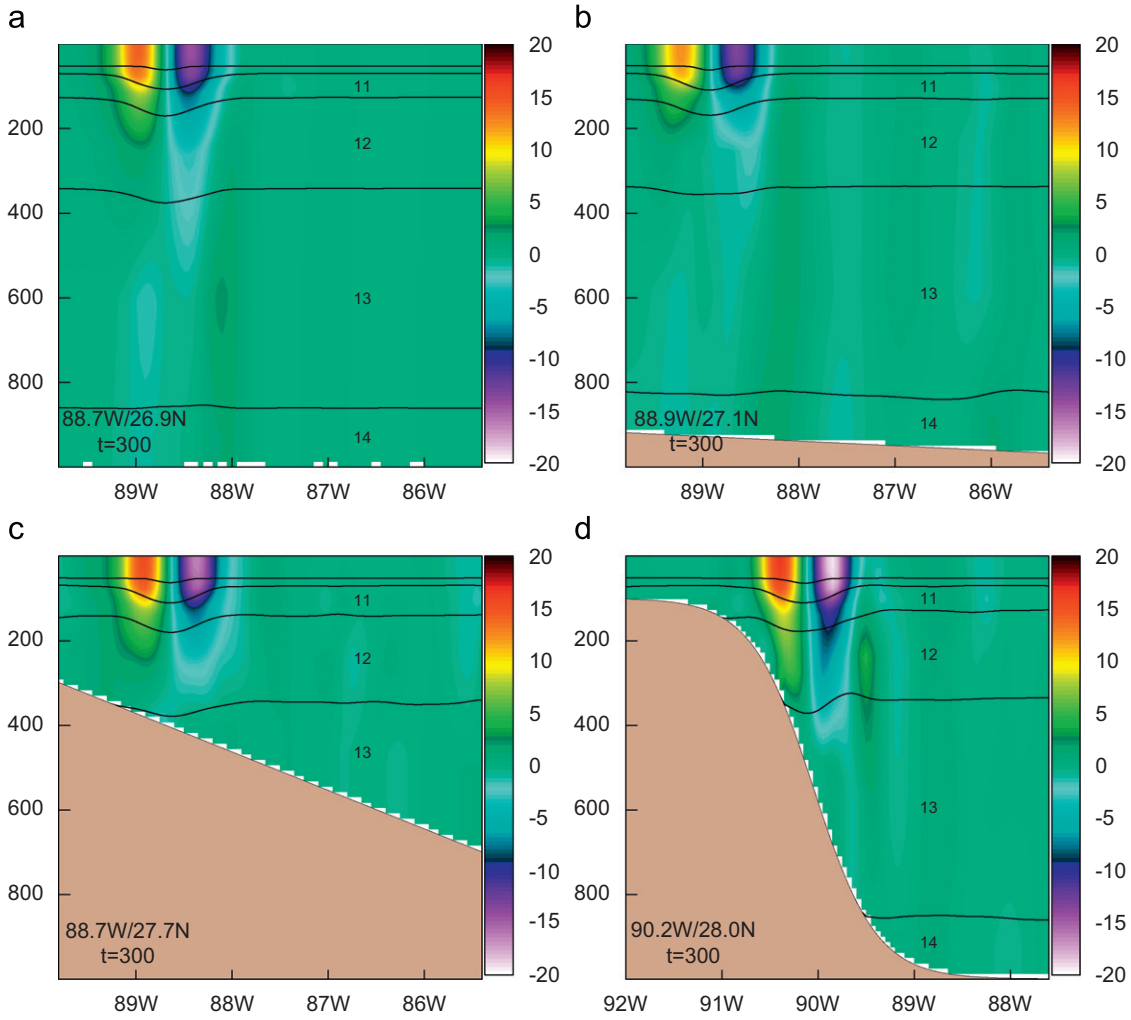

Fig. 6. Zonal section through the vortex center over four topographies (a) B0, (b) W1, (c) W2 and (d) W3, at day 300. Meridional current (color in cm s^{-1}) and layer thickness (line contour) are depicted. The longitude and latitude of the vortex center is given on each panel.

translation is more zonal, and the meridional translation is weaker (~0.3 km day^{-1}) than the weak slope case (W1). This result implies that the deep current is instrumental in driving the zonal/meridional translation when the vortex is situated over a flat bottom or gentle slope, and that the tendency to tilt upslope increases the zonal translation and slightly decreases the meridional translation over a gently sloping bottom, which is consistent with most observed oceanic vortices.

3.2. *Effects of the slope orientation*

Fig. 8 depicts the trajectory of the surface vortex for the flat bottom case (B0) and cases with an eastern, western, southern and northern slope (cases E2/W2/S2/N2). This vortex is strongly affected by topographic β during the early period when the vortex maintains barotropic structure. Note that the first 2–4 dots are down slope from the initial position, in Fig. 8. During this period, the planetary β-gyre dynamics is not fully developed and topographic β (7×10^{-11} s^{-1}) dominates planetary β (2×10^{-11} s^{-1}). The initial down slope drift is the strongest over the northern slope because planetary and topographic β's are in the same direction (note that the first four dots are due southward for N2, in Fig. 8). Once the β-gyre is generated after ~30 days and the vortex weakens the deep currents planetary β effect starts to overcome topographic constraint (e.g. onshore translation in W2) subsequently.

The overall vortex translation is fastest for B0 and slowest for N2. All slope cases have a slower meridional translation than B0. Excluding B0, the vortex translation is fastest for E2 and slowest for N2. In terms of meridional translation, B0 is the fastest and S2 is the slowest. Slow translation for N2 is opposite to that reported by Jacob et al. (2002), who suggested that a northward-sloping topography increased the propagation speed because both planetary and topographic β effects were in the same direction, which is discussed in more detail below. The meridional translation is stronger over the meridional slopes (i.e. isobaths in meridional direction: cases E2, W2) than the zonal slopes, where the zonal translation is dominant. For the meridional slope cases, the southward component is relatively strong in E2 and the westward component is relatively stronger in W2. For the zonal slope cases, the southward component is relatively strong in N2 and the westward component is strong in S2.

The difference in vortex translation due to the slope orientation is caused by the location of adjacent cyclones to the surface vortices. Fig. 9 depicts horizontal vortex evolution for cases E2, W2, S2 and N2 at day 300. In all cases, a cyclone was generated early on the right-hand side of the slope due to topographic β (for an observer looking onshore), resulting in initial down slope drift (see Fig. 8). As the vortex translates southwestward/

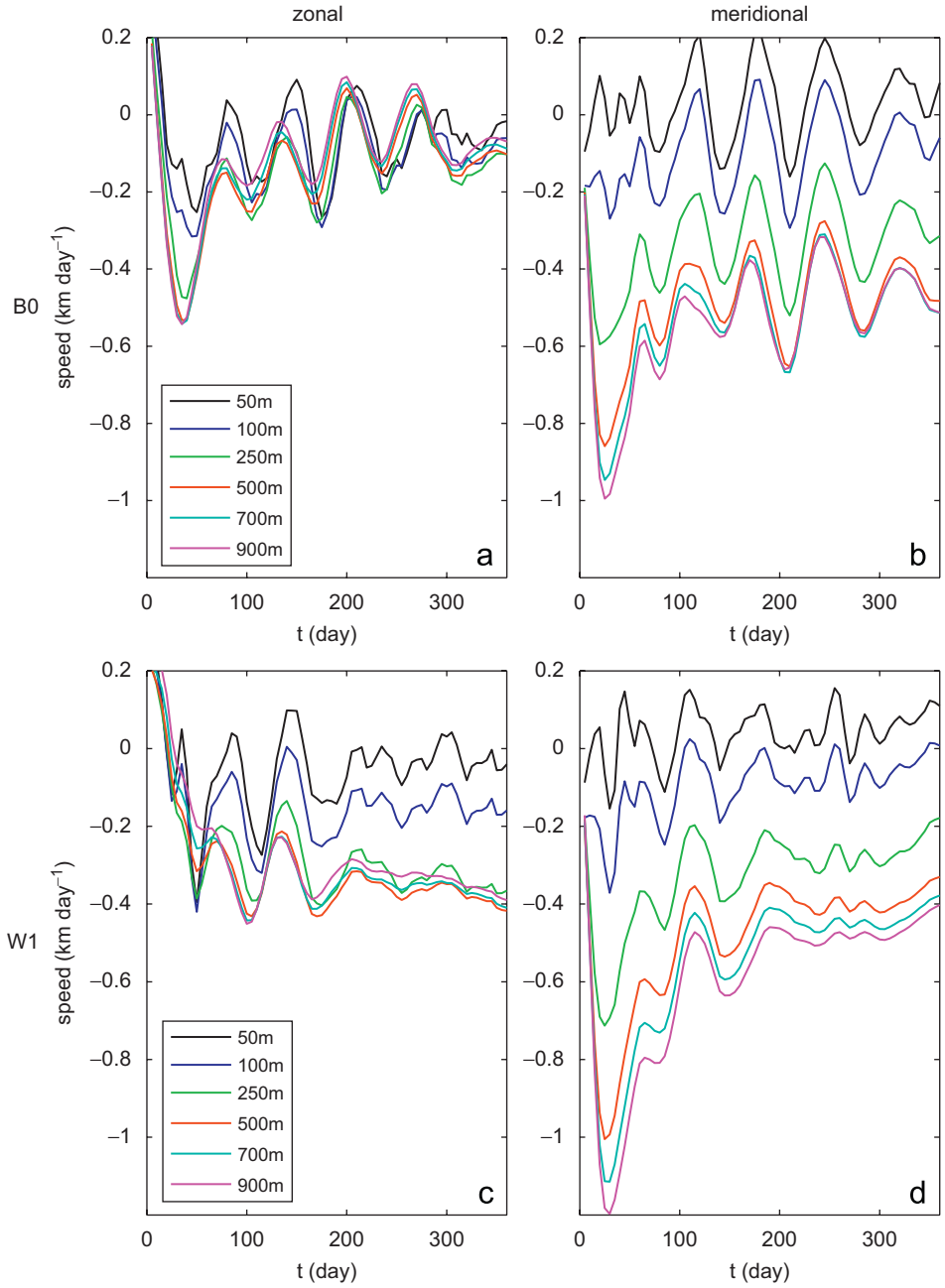

Fig. 7. (a), (c) Zonal and (b), (d) meridional translation speed averaged inside of the vortex for cases B0 (top) and W1 (bottom). Eddy boundary is defined as SSH > 1 cm, and translation speed is averaged from the surface to each depth.

westward, the cyclone is located to the east due to β_0 effect and onshore due to β_τ effect. Thus for E2, W2, S2 and N2, the center of the cyclone is located northeast/northeast/east/northeast and north of the vortex core, respectively. Note that in cases E2/S2/N2, a branch of the cyclone is located between the vortex and the onshore side of the slope (Fig. 9a, c, d), and in case W2, a cyclone is located south and north of the vortex (Fig. 9b). The combined translation of the surface vortices is strongly accelerated due to the presence of these cyclones. The cross-slope translation component is stronger for N2 than S2 because southward translation is retarded by the downslope translation tendency of anticyclones. This suggests that slower meridional translation in S2 is due to topographic constraint. In N2, the β effect is enhanced due to combined effect of planetary and topographic β. However the translation is the slowest of all, which indicates that a larger β effect hinders vortex translation (Fig. 9d). In essence, the cyclone north of the vortex induces eastward translation and reduces westward translation. In N2, the increased β effect retards southward translation because the vortex tends to maintain a consistent decrease rate of planetary vorticity (f) to balance vortex dissipation (ζ increase) to conserve potential vorticity. By retarding southward translation under a larger β effect, f decreases at a consistent rate with a shorter southward translation than under a smaller β effect.

3.3. *Alongslope deflection by topography*

In this section, the evolution of the surface vortex and the subsequent alongslope deflection by topography for case W2 is described. The southwestward translating vortex W2 deflects slightly alongslope at day 365 when the vortex reaches the

bottom, and interacts directly with topography (Fig. 10b). Note that the deep vortex reaches the slope and strongly distorts at day 365 (Fig. 10b, e) compared to before (day 245, Fig. 10a, d) and after (day 465, Fig. 10c, f). The alongslope deflection is the signature of vortex dispersion via topographic Rossby waves (TRW) by β_τ effect. Recall that the TRW propagates toward the south in the western slope case. The vortex collision generates a cyclone south of the impact point (88.4°W, 27.6°N at day 245 in Fig. 10a; 89.1°W, 27.1°N at day 365 in Fig. 10b) ("collision cyclone" hereafter). This cyclone is not generated by topographic β, but rather by the collision of the onshore swirl current of the vortex against the slope. Note that the onshore current turns south, generating a strong slope jet and a cyclone south of the vortex at day 365 (Fig. 10b). The cyclone before and after day 365 is weaker (Fig. 10a, c), indicating weaker interaction with topography. In the weak slope case (W1), neither the collision nor the cyclone occurs because there is no direct interaction between the vortex and topography (see Fig. 5b). The 'collision' cyclone is important in the steep slope case, where the vortex impinges the slope strongly and the shelf-slope front is clear (described in further detail in Section 3.4.2).

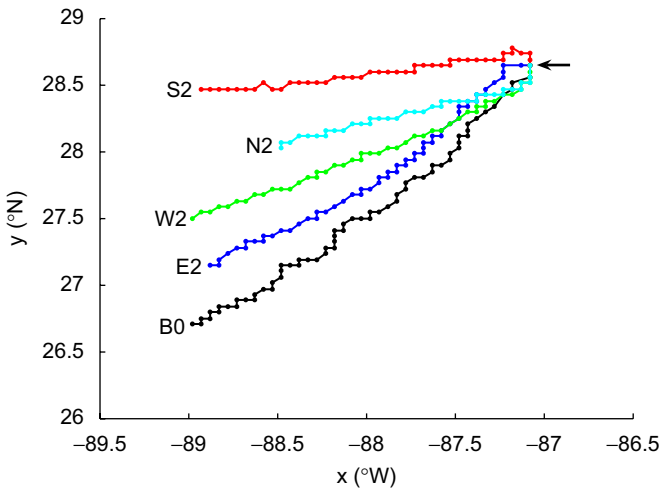

Fig. 8. Vortex trajectory over the eastern, western, northern, southern slopes (cases E2, W2, N2 and S2) and a flat bottom (B0) for 1 year. Initial location is denoted by arrow, and trajectory is depicted by dots every 5 days.

The deflection point can be detected by the variation in relative vorticity in the bottom layer, as shown in Fig. 11, which exhibits time series of relative vorticity in the bottom layer (within 100 m above the bottom), following the center of the vortex, and the zonal translation. A peak of anticyclonic vorticity occurs near day 360 when the vortex deflects alongslope, which matches the peak of anticyclonic vorticity. Fig. 11 also shows that vorticity

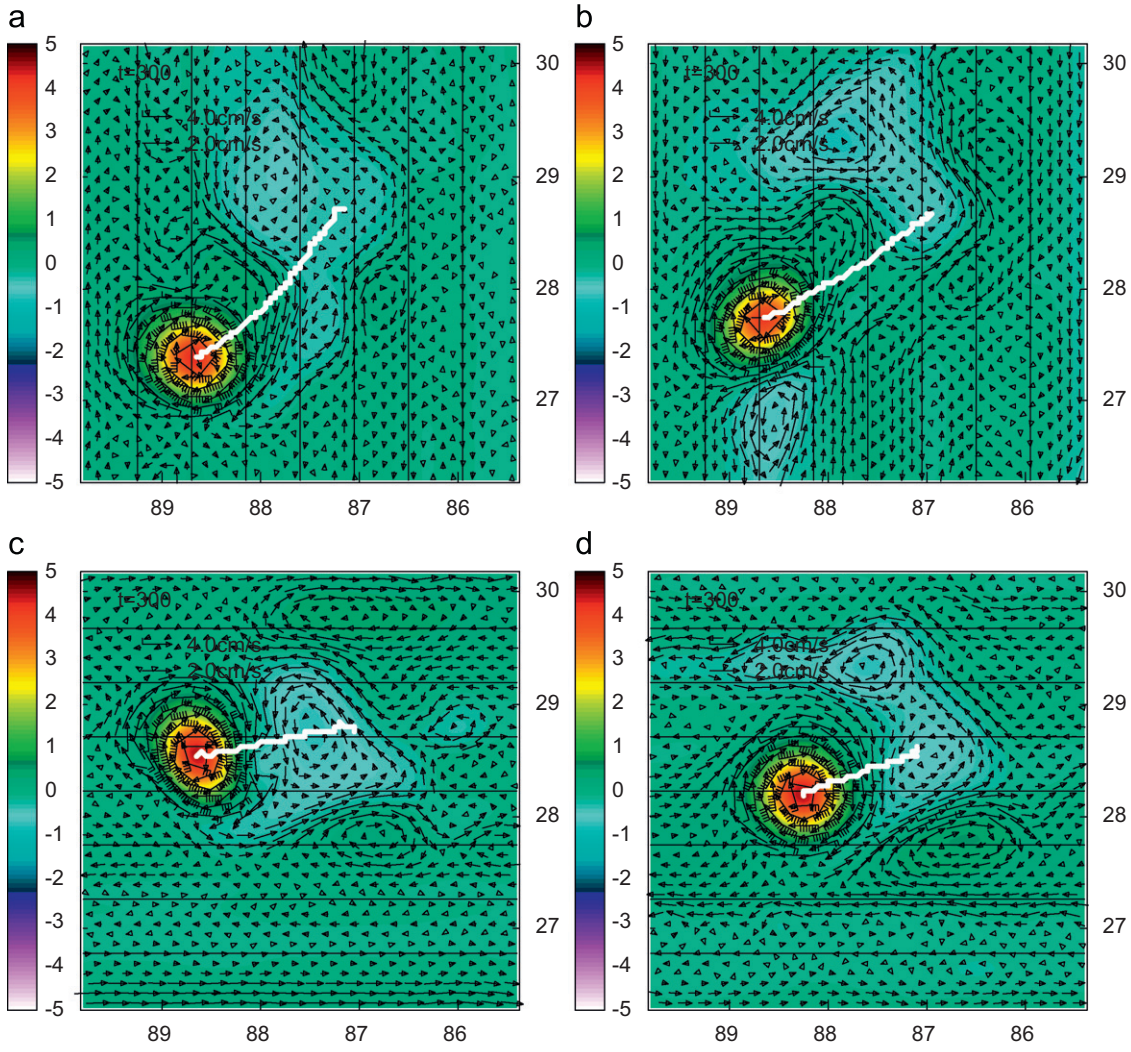

Fig. 9. Vortex evolution over the eastern, western, northern, southern slope (cases E2, W2, S2, N2, respectively) at day 300. SSH (color in cm), layer 10 currents (vectors) and trajectory of the vortex center (white line) are depicted. Bathymetry is superimposed every 50 m.

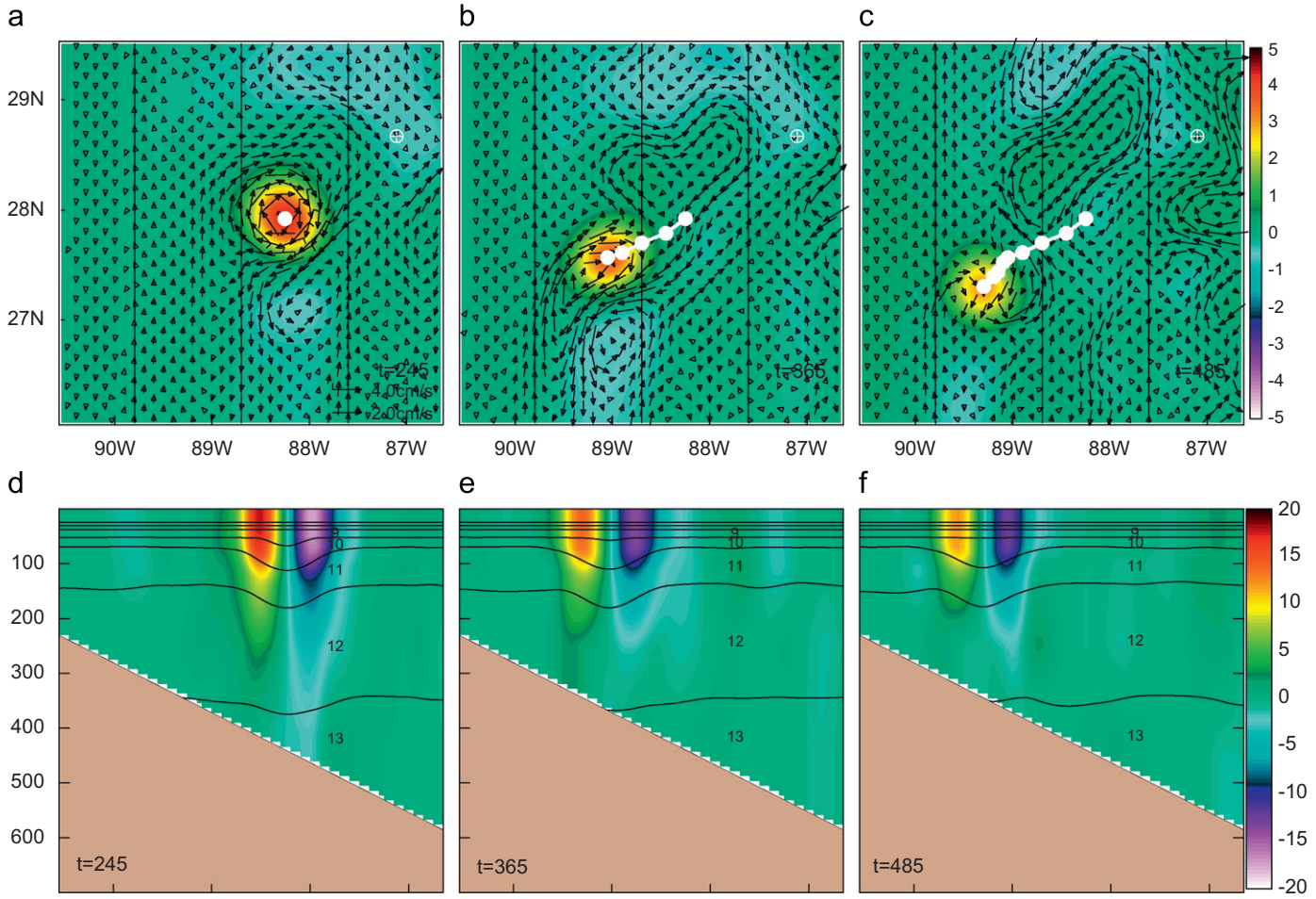

Fig. 10. Vortex drift over an intermediate slope (W2). Horizontal plot is SSH (above) superimposed by the lower-layer current in layer 12. White dots mark the trajectory of the vortex center at every 30 days. The meridional flow (cm s^{-1}) sectioning the center of the vortex is depicted with the layer thickness (below).

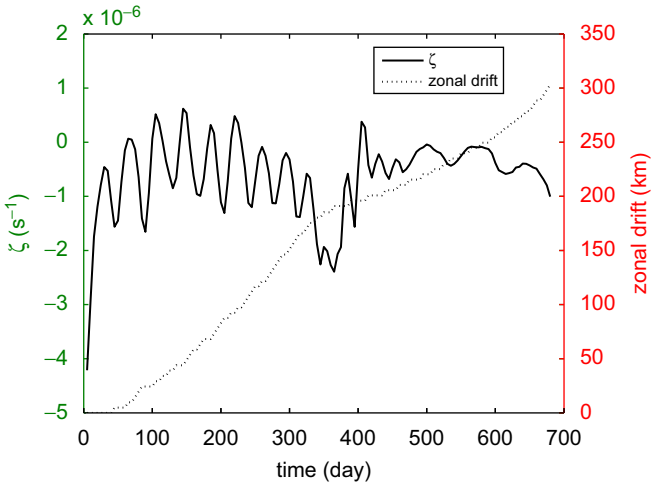

Fig. 11. Time series of the zonal drift (dotted line) and relative vorticity (ζ) in the bottom layer (within 100 m above the bottom) below the vortex center (case W2).

oscillation coincides with the repetition of alongslope and cross-slope oscillations (stepwise curve of zonal translation) before the deflection. Alongslope/cross-slope translation and the decrease/increase in anticyclonic vorticity occur simulataneously, which indicates that the vortex drifts alongslope as it decays and cross-slope as it gains strength (which will be discussed further in Section 3.4.3). The vortex however generally drifts southwestward because the slope is relatively gentle, and shoals continuously. These results suggest that the vortex tends to adjust to a 'compensated' state (zero deep flow) after colliding with the topography, and that the strength of the deep current prior to impact determines the degree of interaction, similar to that reported in Agulhas rings (Kamenkovich et al., 1996). The collision effect is amplified when the vortex is drifting toward the steep slope, as described in Section 3.4.2.

3.4. *Vortex evolution: the steep slope case*

3.4.1. *Evolution of vortex due to initial location from the slope*

Vortex–slope interaction and evolution can differ based on several factors; in this section, vortex behavior is examined as a function of its initial location with respect to the slope. Fig. 12 depicts vortex evolution via tracer distribution for four cases. The first is the flat bottom case (B0, Fig. 12a), the other three cases are W3, W4 and W5, which have the initial vortex location progressively further from the western slope (Fig. 12b–d) (see Table 1). As shown in Fig. 12, significant differences due to the initial location are evident in the vortex trajectory. W3 exhibits an alongslope translation for the entire period (Fig. 12d), while W4 exhibits a zonal translation initially and subsequently alongslope translation (Fig. 12c). W5 undergoes a cross-slope trajectory with a short northward translation in the middle of the slope, after

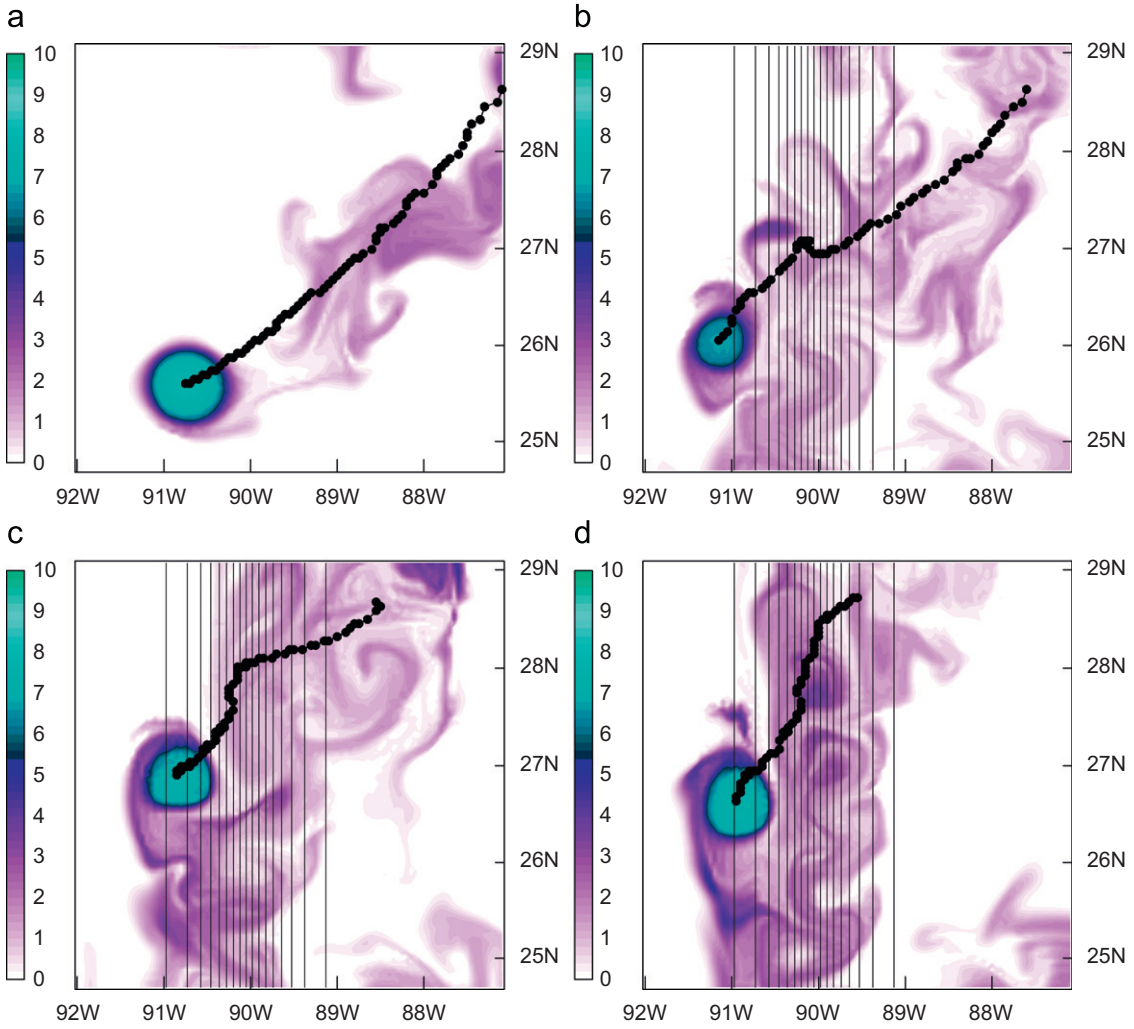

Fig. 12. Passive tracer distribution after 2 years for cases (a) B0, (b) W5, (c) W4 and (d) W3. Trajectory of the vortex center is depicted every 10 days, denoted as dots. Initially, tracer concentration was set to 10 inside of the vortex and zero outside. The tracer is not influenced by diffusion but by advection. Bathymetry is superimposed every 50 m starting 100 m.

southwestward translation on the flat bottom (Fig. 12b). W3 exhibits a dominant alongslope translation over the slope, but cross-slope translation is dominant in W5. Here, W3 is classified as an alongslope drifting vortex and W5 as cross-slope drifting vortex. W4 is the intermediate case between the two, exhibiting an alongslope deflection in the middle of the slope after the initial cross-slope translation. The cross-slope to alongslope deflection angle in W4 is much sharper than in case W2 (see Fig. 10), representing a stronger topographic constraint of the steep slope. W5, the case with strongest westward inertia, is not constrained by the topography and crosses the slope more quickly than W3 and W4.

The tracer distribution clearly displays the vortex-induced mixing and cross-shelf exchange. When the vortex impinges the slope, a filament is generated on the onshore side first (not shown), indicating that the onshore side of the vortex is distorted by the topography. Subsequently, the onshore filament rotates clockwise and generates strong mixing. In all cases with topography, the tracer distribution covers a much larger area than the case with the flat bottom. Note that the vortex tracer is widely distributed over the slope, and further to the south of the vortex (Fig. 12c, d). The final vortex destination is on-shelf for cases W3–W5, which suggests that oceanic vortices can cross the steep slope. W5 reaches the shelf earliest even though it was initialized farthest offshore. Total tracer concentration accumulated at the shelf (<150 m) reveals that about 23%, 15%, and 13% of the initial vortex cross the shelf break in W3, W4, W5, respectively, after 2 years of translation. An experiment without the continental shelf (not included) was performed in order to see whether the vortex translates northward along the western boundary by the 'image effect' (Sutyrin et al., 2003). That case exhibited continuous southward translation along the boundary with enhanced dissipation.

3.4.2. *Effect of strong collision*

In the previous section, it was noted that case W5, although initialized farthest from the slope, impinged upon the shelf earlier than other cases. It also traversed the width of the slope more quickly than other cases. In this section, we examine the evolution of the trajectory and vertical deformation of case W5 in greater detail. Fig. 13 illustrates the evolution of the vortex in case W5, exhibiting a relatively strong westward inertia, and crossing the steep slope more rapidly than other cases. This cross-slope drifting vortex generates a divergence and a 'collision' cyclone to the south (Fig. 13a–c), and experiences strong distortion and erosion (see Fig. 13c–f). This cyclone is much stronger than W3 and W4 due to the stronger collision. The vortex translates nearly zonally before the collision (Fig. 13b) and drifts poleward for a short period of time (Fig. 13c). The poleward drift is generated as

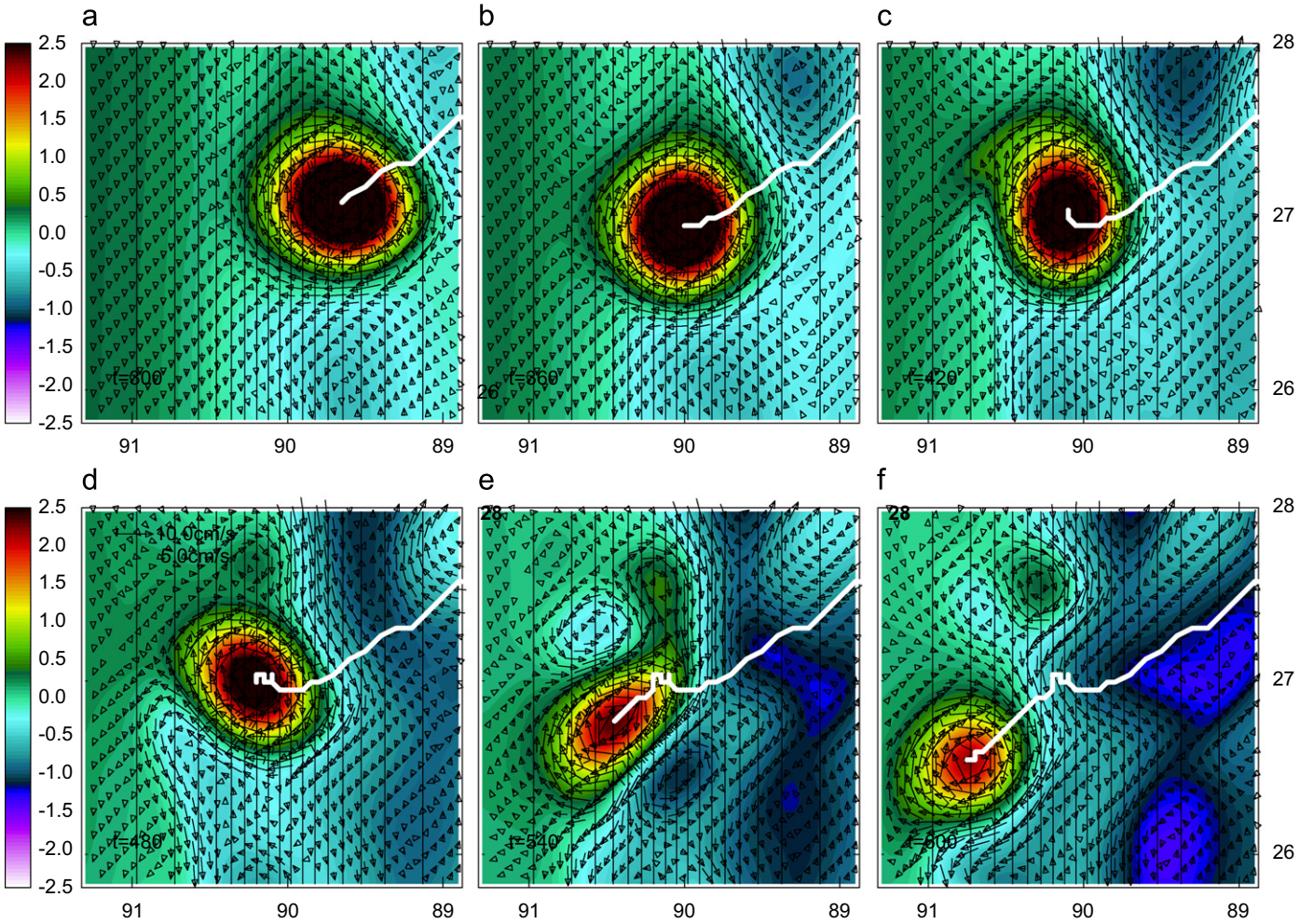

Fig. 13. Evolution of the vortex crossing a steep slope (case W5). Current in layer 10, SSH and trajectory of the vortex center are depicted from 300 to 600 days with 60 days interval.

the vortex rotates clockwise (Fig. 13c) and is likely caused by the "image effect", the tendency of the zonally compressed vortex drifting along the wall as if there were an opposite sign of vortex on the other side (Shi and Nof, 1993; Sutyrin et al., 2003). Similar poleward motion for anticyclones was also reported in the LCE by Kirwan et al. (1988) and in North Brazil current rings (Fratantoni et al., 1995). The vortex compression can be clearly seen in the sectional view (Fig. 14). The onshore part becomes over-compressed by the strong collision and is located further onshore (Fig. 14b, c), and the over-compressed northward branch produces a net poleward translation, which is the state of the peak of collision. However, the poleward drift here is fairly short and is not persistent. Recall that an experiment with a close western boundary without the continental shelf (not included) did not exhibit a northward translation along the boundary. These results, therefore, suggest that persistent northward translation is not generated only by vortex–boundary or vortex–slope interaction, but by other dynamics such as vortex–vortex interactions or regional currents.

The divergence and the 'collision' cyclone south of the vortex are typical phenomena as the vortex impinges upon the western slope (Fig. 13a, b), and do not clearly occur over eastern/southern/northern slopes due to the westward translation tendency (see Fig. 9). This cyclone was seen in the intermediate slope case (Figs. 9 and 10), but more weakly than in the steep slope case. Frolov et al. (2004) suggested that the cyclone generated north of the vortex by the topographic β enhanced an offshore reflection. Typically, ocean cyclones are observed both south and north of vortices which impinge upon the western slope. For example, Vidal et al. (1994) reported an anticyclone's interaction with the western GoM continental slope originated flanking cyclonic rings to the north and south of the colliding anticyclone. In cases where the vortex impinges strongly upon the western slope (which occurs more frequently in the GoM than the vortex initially over the northern slope, reported by Oey and Zhang (2004)), the 'collision' cyclone and the slope jet to the south would be stronger (as seen in Fig. 13).

Due to strong vortex–topography collision, the vortex undergoes enhanced erosion, as described below. Such vortex erosion and northward isolation of the cyclone can be seen in Fig. 14c–f. A branch of the 'collision' cyclone which translates to the north of the vortex plays a significant role in horizontal erosion. Note that the impinging vortex distorts at day 540 and erodes into two vortices at day 600. The 'collision' cyclone, extended onshore (Fig. 13d) and located north of the vortex (Fig. 13e), erodes the northern filament of the vortex (Fig. 13e, f). Simultaneously, vertical erosion occurs i.e. the lower part of the vortex is eroded and becomes slender near the topography (Fig. 14c–e). Between days 480 and 540, the onshore part of the vortex is nearly eroded in layer 12 (Fig. 14d, e), as is the offshore segment at day 600 when the vortex translates onto the shelf (Fig. 14f). This vertical erosion is a common process as the vortex crosses the steep topography.

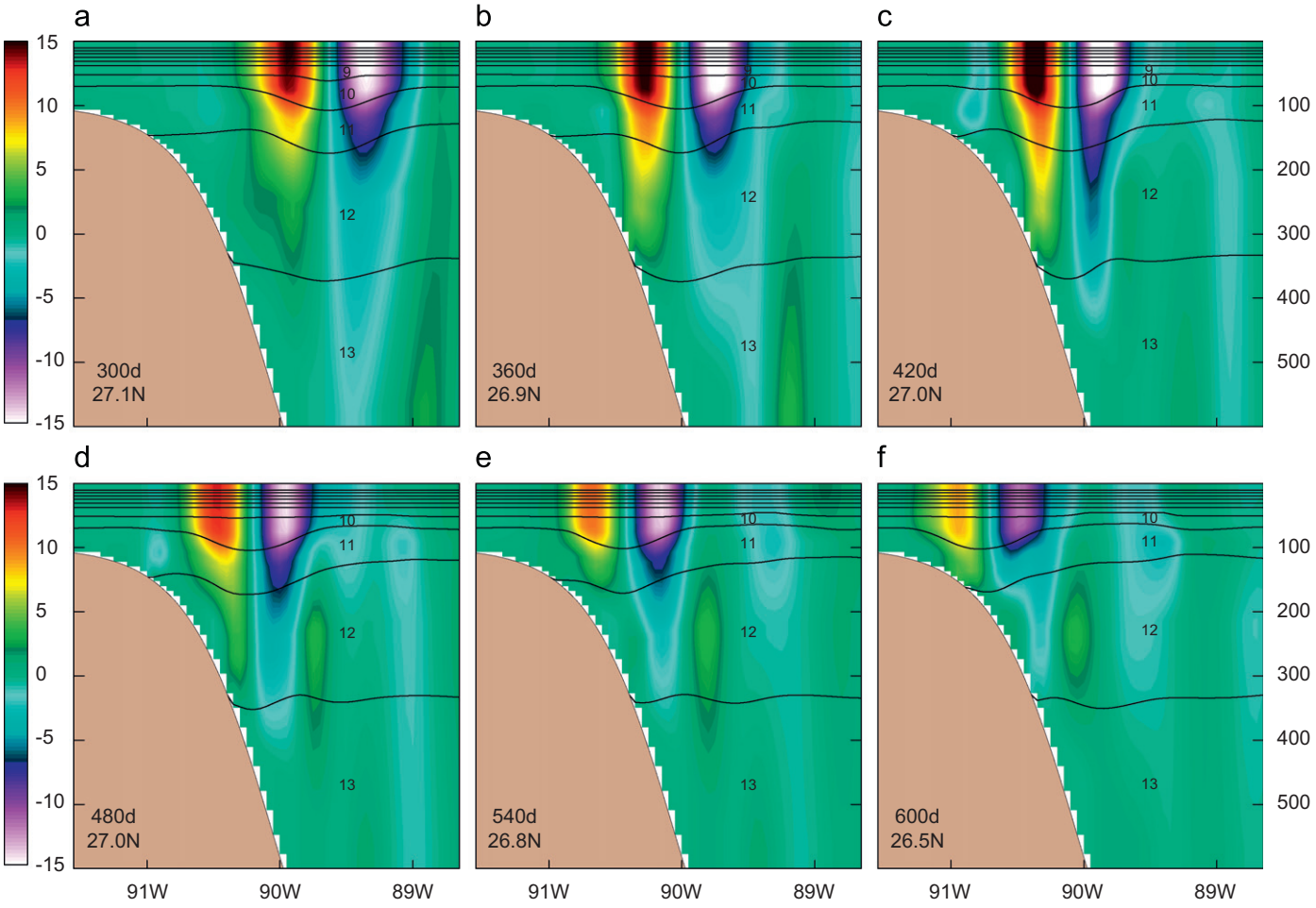

Fig. 14. Zonal section of the vortex crossing the steep slope (case W5). Meridional current and layer thickness are depicted from 300 to 600 days with 60 days interval. Latitude of the center is given on each panel.

As the vortex erodes horizontally and vertically, it shoals rapidly and restores southwestward translation (Figs. 13d–f and 14d–f).

3.4.3. *Vorticity variation during vortex–topography collision*

The vortex–topography collision can be detected by vorticity variation over a slope. Fig. 15 depicts a time series of vorticity following the vortex center. In the flat bottom case, the vortex decays with time by losing negative vorticity in the lower layer. Note that the vorticity below 200 m decreases rapidly compared to the nearly constant surface vorticity, for the first 250 days. The collision effect can be seen as the surface vorticity (denoted by white line) stretches and generates a 'bulge' shape over the slope at ~450 days, which indicates an increase in the total anticyclonic vorticity and downward momentum transfer. A vortex experiencing a gradual adjustment over a slope (e.g. W2, W3) exhibited a slight increase of vorticity without a 'bulge' shape (not shown). The 'bulge' shape is only formed for case W5 and is a signature of strong collision. The peak of this shape coincides with the turning point from northward to southward translation (f increase to decrease).

Vorticity variation over a steep slope can be described by a vorticity balance between ζ and f (Fig. 16). In general, the vortex conserves potential vorticity on a flat bottom without diffusion, i.e.

$$Q = (f+\zeta)/h = (\text{decrease} + \text{increase})/(\text{constant}) = \text{constant}$$

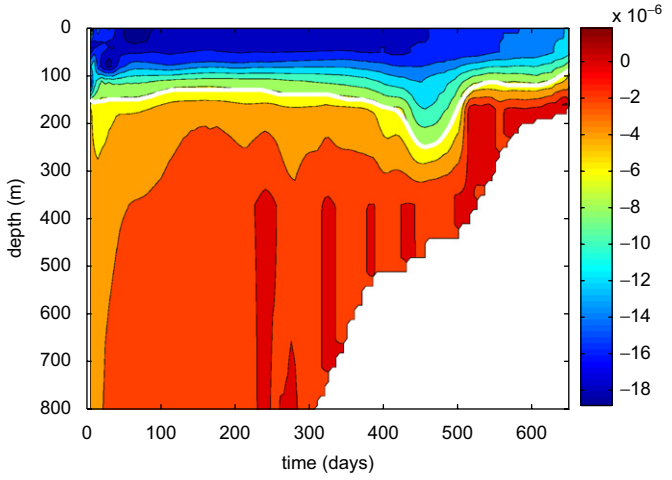

Fig. 15. Time series of relative vorticity (s^{-1}) at the vertical axis of the vortex center (case W5). Thick white line indicates a vorticity of $-6\times10^{-6}\,s^{-1}$.

since it loses negative vorticity (ζ increase) and subsequently drifts equatorward (f decrease). Note that Q is conserved for the first 240 days in the flat bottom region, since ζ and f almost balance each other. However when the vortex translates over a slope, it undergoes both an increase and decrease in relative vorticity. Over the lower slope (days 250–480), the potential

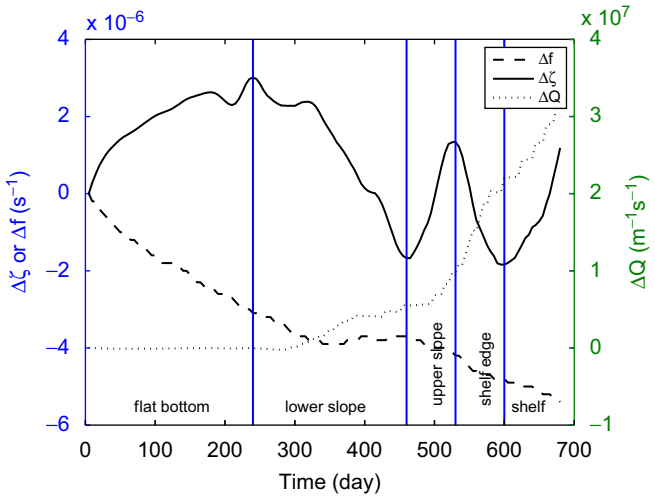

Fig. 16. Time series of vorticity anomalies of planetary (Δf), relative ($\Delta\zeta$) and potential vorticities (ΔQ), for case W5. Relative vorticity was obtained from the depth-averaged current at the vortex center.

vorticity increases gradually as the water column (h) shoals, southward translation decreases (see slow decrease of or constant f) and relatively vorticity (ζ) decreases rapidly (gaining anticyclonic vorticity), i.e.,

$$Q = (f+\zeta)/h = (\text{increase} + \text{decrease})/(\text{decrease}) = \text{increase}.$$

As the vortex gains strength (ζ decrease), it tends to turn westward (slow f decrease rate; zonal dominance). The vortex restores the initial vorticity as it translates poleward (see day 400). Subsequently, it turns south (vorticity dissipation) after the vorticity peaks at day 470 (northern limit). Thus the poleward translation is the signature of vorticity restoration. Over the upper slope (days 480–520), the vortex starts to lose vorticity (ζ increase) and translates southward. A gain in vorticity occurs as the vortex cross the shelf edge (days 520–600). If the vortex loses negative vorticity (ζ increase by dissipation), it translates southward (f decrease). This is similar to the flat bottom region but the water column continuously shoals. The vortex does not directly interact with the bottom during this period. Hamilton et al. (1999) reported that a feature of some mature LCEs in the GoM was their almost constant ζ, and that the absolute vorticity (ζ+f) tended to increase between the central and western GoM, which indicated vorticity restoration. Here, ζ recovers and exceeds the initial values past day 360 after gaining negative vorticity. Over the flat bottom, there is no way to restore vorticity once the anticyclone starts to dissipate and drift equatorward. This result suggests that it is possible for (ζ+f) to decrease slowly or increase if the vortex restores over the slope and the meridional translation is very slow, and that the vortex translates poleward if the vortex restores initial vorticity.

4. Summary

HYCOM is used to investigate topographic effects of the slope steepness and orientation on the evolution of an isolated anticyclonic vortex. In particular, vortex evolution over a steep slope is enlightened with respect to vortex collision, erosion and vorticity restoration. Experiments with a flat bottom, three western slope configurations and an intermediate slope in each slope orientation are analyzed with vortex trajectory, SSH, horizontal and vertical current fields and vorticity. The simulation with the flat bottom exhibits that the counter-rotating vortex, initially generated by the "β-gyre" dynamics and subsequently isolated into the deep layer (deep cyclone), generates a strong equatorward translation. The vortex translates on the flat bottom ocean approximately at the long Rossby wave speed, which is consistent with results from quasi-geostrophic (QG) models (e.g. McWilliams et al., 1986). However, the effect of topography differs significantly from reduced-gravity and QG models because the trailing deep cyclone is strongly affected by the topography. For example, in the weak western slope case, the deep cyclone accelerates the zonal translation due to the tendency to tilt upslope compared to the flat bottom case and enhanced dispersion of the cyclone. The deep cyclone becomes more dispersive as the slope increases, resulting in a dominant zonal translation over the slope until the vortex deflects alongslope. As the vortex collides against a steeper slope and deflects alongslope simultaneously, a 'collision' cyclone and an associated divergence with a slope jet are generated south of the vortex due to the collision of the onshore swirl flow. Over a steep slope, intensified vortex collision and a sharp alongslope deflection occur due to stronger topographic constraint, and the vortex experiences enhanced distortion and erosion. Horizontal and vertical erosions occur as a branch of the "collision" cyclone translates northward and subsequently erodes a filament of the distorted vortex. Vorticity can be restored by vortex–topography collision against a steep topography, which compresses the vortex column strongly and turns it poleward simultaneously. However, persistent poleward translation is not likely generated by vortex–topography/boundary interaction (so called the 'image' effect). Poleward translation along the western boundary has been simulated in a barotropic model (Shi and Nof, 1993) and a two-layer intermediate equation model (Sutyrin et al., 2003). In our model, poleward translation is fairly short over the slope and does not appear along the western boundary. This result implies that poleward translation along the western boundary can possibly occur by other dynamics such as forcing, regional currents and vortex–vortex interactions.

The slope orientation strongly affects the vortex translation due to the location of adjacent cyclones, which tend to translate onshore and poleward simultaneously, enhancing the translation to the combined direction. This study suggests that combined planetary and topographic β effects do not accelerate the vortex translation. It has been widely acknowledged that stronger β effect generates faster vortex translation in both meridional and zonal directions (e.g. Jacob et al., 2002). Instead, the translation decreases as the β effect increases because of vortex's tendency of maintaining relatively constant vortex dissipation rate. The slowest vortex translation over a northern slope suggests that increased β effect does not accelerate translation speed, but reduces both the zonal translation by the cyclone north of the vortex and the meridional translation to balance vortex dissipation for potential conservation.

This paper suggests that the absolute vorticity can decrease slowly or increase if the vortex strength restores over the slope and the meridional translation is very slow, and that the vortex translates poleward if it fully restores initial strength. In short, the vortex, which experiences the dispersion of the deep cyclone but does not contact topography, translates upslope (enhanced zonal translation). On the other hand, the vortex which directly contacts the topography deflects alongslope, generates a slope jet and a 'collision' cyclone to the south and experiences strong vortex distortion and erosion.

Acknowledgments

This work is a contribution to the 6.1 project "Shelf to Slope Energetics and Exchange Dynamics" sponsored by the Office of

Naval Research under program element 0601153 N. It is also a contribution to the 6.2 project "Coastal Ocean Nesting Studies", also sponsored by the Office of Naval Research under program element 0601153 N. We would like to thank Dr. Alan Wallcraft (NRL) for his assistance with HYCOM and useful comments. We would also like to thank Dr. Steven Herbette (UMR) for providing the source code used for the vortex initialization.

References

Bleck, R., 2002. An oceanic general circulation model framed in hybrid isopycnic-cartesian coordinates. Ocean Modeling 4, 55–88.

Bleck, R., Boudra, D., 1981. Initial testing of a numerical ocean circulation model using a hybrid (quasi-isopycnic) vertical coordinate. Journal of Physical Oceanography 11, 755–770.

Brown, O.B., Cornillion, P.C., Emmerson, S.R., Carle, H.M., 1986. Gulf Stream warm rings: a statistical study of their behavior. Deep-Sea Research 33, 1459–1473.

Byrne, D., Gordon, A., Haxby, W., 1995. Agulhas vortices: a synoptic view using geosat ERM data. Journal of Physical Oceanography 25, 902–917.

Carnevale, G.R., Kloosteriziel, R.C., van Heijst, G.J.F., 1991. Propagation of barotropic vortices over topography in a rotating tank. Journal of Fluid Mechanics 233, 119–140.

Carton, X., Williams, J.C.M., 1989. Barotropic and baroclinic instabilities of axisymmetric vortices in a quasigeostrophic model. In: Nihoul, J., Jamart, J. (Eds.), Mesoscale/Synoptic Coherent Structures in Geophysical Turbulence. Oceanography Series. Elsevier, Amsterdam, pp. 225–244.

Chassignet, E.P., Cushman-Roisin, B., 1991. On the influence of a lower layer on the propagation of nonlinear oceanic eddies. Journal of Physical Oceanography 21, 939–957.

Chassignet, E.P., Hurlburt, H.E., Smedstad, O.M., Halliwell, G.R., Hogan, P.J., Wallcraft, A.J., Baraille, R., Bleck, R., 2007. The HYCOM (HYbrid Coordinate Ocean Model) data assimilative system. Journal of Marine System 65, 60–83.

Cheney, R.E., Richardson, P.L., 1976. Observed decay of a cyclonic gulf stream ring. Deep-Sea Research 23, 143–155.

Flierl, G.R., 1977. The application of linear quasigeostrophic dynamics to Gulf Stream rings. Journal of Physical Oceanography 7, 365–379.

Flierl, G.R., 1984. Rossby wave radiation from a strongly nonlinear warm eddy. Journal of Physical Oceanography 14, 47–58.

Fratantoni, D.M., Johns, W.E., Townsend, T.L., 1995. Rings of the North Brazil current: their structure and behavior inferred from observations and a numerical simulation. Journal of Geophysical Research 100 (C6), 10633–10654.

Frolov, S.A., Sutyrin, G.G., Rowe, G.D., Rothstein, L.M., 2004. Loop current eddy interaction with the western boundary in the Gulf of Mexico. Journal of Physical Oceanography 34 (10), 2223–2237.

Grimshaw, R., Broutman, D., He, X., Sun, P., 1991. Analytical and numerical study of a barotropic eddy on a topographic slope. Journal of Physical Oceanography 24, 1587–1607.

Hamilton, P., Fargion, G.S., Biggs, D.C., 1999. Loop current eddy paths in the western Gulf of Mexico. Journal of Physical Oceanography 29, 1180–1207.

Herbette, S., Morel, Y., Arhan, M., 2003. Erosion of a surface vortex by a seamount. Journal of Physical Oceanography 33, 1664–1679.

Herbette, S., Morel, Y., Arhan, M., 2005. Erosion of a surface vortex by a seamount on the β-plane. Journal of Physical Oceanography 35, 2012–2030.

Hurlburt, H.E., Thompson, J.D., 1980. A numerical study of loop current intrusions and vortex shedding. Journal of Physical Oceanography 10, 1611–1631.

Jacob, J., Chassignet, E., Dewar, W., 2002. Influence of topography on the propagation of isolated eddies. Journal of Physical Oceanography 32, 2848–2869.

Kamenkovich, V.M., Koshlyakov, M.N., Monin, A.S., 1986. Synoptic Eddies in the Ocean. D.Reidel Publishing Company, Dordrecht, p. 511.

Kamenkovich, V.M., Leonov, Y.P., Nechaev, D.A., 1996. On the influence of bottom topography on the agulhas eddy. Journal of Physical Oceanography 26, 892–911.

Kirwan, A.D., Lewis, J.K., Indest, A.W., Reinersman, P., Quintero, I., 1988. Observed and simulated kinematic properties of loop current rings. Journal of Geophysical Research 93 (C2), 1189–1198.

LaCasce, J.H., 1998. A geostrophic vortex over a slope. Journal of Physical Oceanography 28, 2362–2381.

Ladd, C., Kachel, N., Mordy, C., Stabeno, P., 2005. Observations from a yakutat eddy in the northern Gulf of Alaska. Journal of Geophysical Research 110, C03003.

Louis, J.P., Smith, P.C., 1982. The development of the barotropic radiation field of an eddy over a slope. Journal of Physical Oceanography 12, 56–73.

Matsuura, T., Kamachi, M., 1993. The evolution of isolated vortices interacted with steep slope. Journal of Oceanography 49, 317–352.

McWilliams, J.C., Flierl, G.R., 1979. On the evolution of isolated, nonlinear vortices. Journal of Physical Oceanography 11, 1662–1672.

McWilliams, J.C., Gent, P.R., Norton, N.J., 1986. The evolution of balanced, low-mode vortices on the β-plane. Journal of Physical Oceanography 16, 838–855.

Mied, R.P., Lindemann, G.J., 1979. The propagation and evolution of cyclonic Gulf stream rings. Journal of Physical Oceanography 9, 1183–1206.

Morrow, R., Birol, F., Griffin, D., Sudre, J., 2004. Divergent pathways of cyclonic and anti-cyclonic ocean eddies. Geophysical Research Letters 31, L24311.

Mory, M., Stern, M.E., Griffiths, R.W., 1987. Coherent baroclinic eddies on a sloping bottom. Journal of Fluid Mechanics 183, 45–62.

Nof, D., 1983. On the migration of isolated eddies with application to Gulf stream rings. Journal of Marine Research 41, 399–425.

Nof, D., 1999. Strange encounters of eddies with walls. Journal of Marine Research 57 (5), 739–761.

Oey, L.-Y., Zhang, H.C., 2004. The generation of subsurface cyclones and jets through eddy–slope interaction. Continental Shelf Research 24, 2109–2131.

Robinson, A.R., 1983. Eddies in Marine Science. Springer, Berlin, p. 609.

Shi, C., Nof, D., 1993. The splitting of eddies along boundaries. Journal of Marine Research 51, 771–795.

Smith IV., D.C., 1986. A numerical study of loop current eddy interaction with topography in the western Gulf of Mexico. Journal of Physical Oceanography 16, 1260–1272.

Smith IV., D.C., Reid, R.O., 1982. A numerical study of non-frictional decay of mesoscale eddies. Journal of Physical Oceanography 12, 244–255.

Smith IV., D.C., O'Brien, J.J., 1983. The interaction of a two-layer isolated mesoscale eddy with bottom topography. Journal of Physical Oceanography 13, 1681–1697.

Sutyrin, G.G., Rowe, G.D., Rothstein, L.M., Ginis, I., 2003. Baroclinic eddy interaction with continental slopes and shelves. Journal of Physical Oceanography 33, 283–291.

Teague, W.J., Carron, M.J., Hogan, P.J., 1990. A comparison between the generalized digital environmental model and Levitus climatologies. Journal of Geophysical Research 95 (C5), 7167–7183.

Thierry, V., Morel, Y.G., 1999. Influence of a strong bottom slope on the evolution of a surface intensified vortex. Journal of Physical Oceanography 29, 911–924.

Vidal, V.M.V., Vidal, F.M., Perez-Molero, J.M., 1992. Collision of a loop current anticyclonic ring against the continental shelf slope of the western Gulf of Mexico. Journal of Geophysical Research 97 (C2), 2155–2172.

Vidal, V.M.V., Vidal, F.V., Hernandez, A.F., Meza, E., Perez-Molero, J.M., 1994. Baroclinic flow transports and kinematic properties of a cyclonic–anticyclonic–cyclonic ring triad in the Gulf of Mexico. Journal of Geophysical Research 99, 7571–7597.

Vukovich, F.M., Waddell, E., 1991. Interaction of a warm ring with the western slope in the Gulf of Mexico. Journal of Physical Oceanography 21, 1061–1074.

Wang, G., Dewar, W.K., 2003. Vortex–seamount interactions: implications for the Mediterranean salt tongue. Journal of Physical Oceanography 33, 2446–2461.

Warren, B.A., 1967. Notes on translatory movement of rings of current with application to Gulf Stream eddies. Deep-Sea Research 14, 505–524.

Whitehead, J.A., Stern, M.E., Flierl, G.R., Klinger, B.A., 1990. Experimental observations of baroclinic eddies on a sloping bottom. Journal of Geophysical Research 95, 9585–9610.